Development of an Orbital Angular Momentum Sorter for High-Speed Data Transfer

Intel Science Talent Search
Physics
November 2005

Amol Jain

Herricks High School
New Hyde Park, NY 11040

and

Laser Teaching Center
Stony Brook University
Stony Brook, NY 11794-3800

1 Introduction

There has always been a motivation to increase the pace at which information is transmitted, and light has proved an ideal medium for high-speed data transfer, most notably through fiber optic networks. Recent advances in free-space communication systems, however, have revived interest in optical links outside the sphere of fiber optics [1]. Free-space systems function without wave guides, making them better suited for temporary connections and areas where deploying a fiber optic cable is logistically unfeasible. These links rapidly modulate the intensity, frequency, or polarization of light between two states, representing the 0s and 1s of binary data transfer. Clearly, an augmented alphabet of more than two states would permit much faster transmissions.

Recently, it has been shown that laser light beams can be given a property, orbital angular momentum (OAM), that offers this possibility [2, 3]. In contrast to polarization encoding, the number of possible OAM states of a light beam is limited only by practical considerations. Thus, OAM-encoding can conceivably be used to substantially increase the rate of data transfer over conventional binary methods. Light beams that carry OAM are called optical vortices. They are characterized by a spiral-shaped phase distribution that creates a region of zero field amplitude in the center of the beam [4]. The rate at which the phase advances around the circumference of the beam is proportional to the OAM of its photons [2].

The research described in this report has three principal components related to the overall goal of designing and demonstrating a practical and effective OAM transmission scheme. In the first and most detailed study, an adjustable spiral phase plate was investigated and mathematically modelled to better understand its vortex generation capability. The phase plate is useful even outside the context of this project in that it costs essentially nothing and is 100% efficient, features which may be decisive in applications such as optical tweezers. Second, a composite grid computer-generated hologram (CGH) was developed to analyze the vortices, or measure their OAM. The method used for constructing the CGHs was simpler than previous procedures. Finally, a conceptual design of an OAM sorter based on the two components was proposed and analyzed mathematically.

2 Theory and Background

2.1 Optical Vortices

An optical vortex beam is characterized by a doughnut-shaped intensity distribution with a phase singularity, and hence zero field amplitude, at its center. Optical vortices feature a screw-shaped topological wavefront dislocation, which can be visualized as a helical phase ramp around the field's dark core.

All light beams are solutions to the scalar wave equation:

$$\nabla^2 U - \frac{1}{c^2}\frac{\partial^2 U}{\partial t^2} = 0$$

One family of solutions known as Laguerre Gaussian beams have this form [5]:

$$U_l^p(r,\phi,z) = \exp\left[-\frac{ikr^2}{2R} - \frac{r^2}{w^2} - i(2p+l+1)\psi\right]\exp[-il\phi](-1)^p\left(\frac{r^2}{w^2}\right)^{\frac{l}{2}} L_p^l\left(\frac{2r^2}{w^2}\right)$$

where $R(z) = z\sqrt{1+(z/z_0)^2}$ is the wave-front radius of curvature, $w(z) = w_0\sqrt{1+(z/z_0)^2}$ is the beam radius, ψ is the Guoy phase, and L_n^k is a generalized Laguerre polynomial:

$$L_n^k(x) = \sum_{m=0}^{n}(-1)^m\frac{(n+k)!}{(n-m)!(k+m)!m!}x^m$$

The two indices l and p associated with each mode describe the total phase change around the circumference of the vortex ($2\pi l$) and the number of radial maxima ($p+1$), respectively. The most familiar and commonly occuring laser beams have both l and $p = 0$, resulting in a Gaussian-shaped intensity distribution and a phase that is uniform throughout any plane perpendicular to the direction of beam propogation. If l is non-zero, however, the beam assumes vortex properties.

The distinguishing characteristic of optical vortices is found in the $\exp[il\phi]$ term. The

angle ϕ resides in the plane transverse to the direction of beam propagation and introduces the element of azimuthal variance in LG beams. As ϕ varies from 0 to 2π, the phase of light around the circumference varies linearly and may be calculated by $l\phi$. A suitable analogy is found in the Earth. Looking down upon the north pole, one can see lines of longitude (indicative of the azimuthal angle and, hence, the phase of light) converging upon the center. At the north pole, there is no distinct longitude. Likewise, at the center of an optical vortex, there is a singularity in the phase, and the amplitude of the beam is necessarily zero. This gives rise to optical vortices' dark center and doughnut shaped intensity distribution.

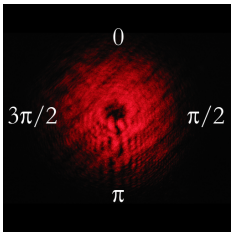

Figure 1: Optical vortex produced by spiral phase plate and phase around circumference.

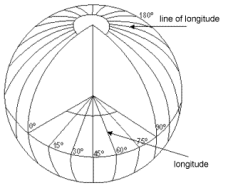

Figure 2: Comparison between the phase in a cross section of an optical vortex and longitude lines at the north pole.

The topological charge of a vortex is another name for its l-value. Connecting all points of equal phase in a charge one vortex creates a helical phase ramp. The locus of points of equal phase in a charge two vortex would produce a double-helix. The same trend holds true for larger l. The size of the dark core of an optical vortex also increases with l.

2.2 Spiral Phase Plates

The various possible means of producing optical vortex beams include intra-cavity circular absorbers, astigmatic mode converters, computer-generated holograms (CGHs), and spiral phase plates. Intra-cavity circular absorbers significantly reduce the intensity of the beam and require access to the laser cavity, rendering them impractical for use in many circumstances. Astigmatic mode converters rely on high-order Hermite-Gaussian modes of certain indices [6], making them more cumbersome to set up. CGHs divide the overall intensity of a light beam into multiple diffraction orders, limiting them in efficiency but making these devices

more suitable for beam analysis [7], as described later in this report.

Spiral phase plates are ideal for vortex production (and many other applications) because the entire beam energy can be concentrated into a single OAM state with 100% efficiency.

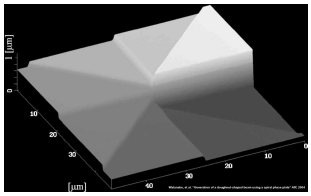

Figure 3: Increasing thickness translates to increased optical path length and a phase shift.

Spiral phase plates function by directly imposing a phase shift distribution on an incident light beam. In the traditional, fixed form, they are constructed by shaping a piece of transparent material in such a way as to have a gradually increasing, spiraling thickness. Light slows down in optically dense media, taking more time to cover a given distance inside the media than outside in air. It simplifies matters, however, to approach phase shift in terms of distance rather than time. Thus the idea of the optical path length (OPL), the apparent distance light travels in any medium is defined:

$$\Lambda = \int n(s)ds$$

where n, the index of refraction, is a function of distance s. The thicker the plate, the longer the optical path length, and the greater the phase shift. The spiraling thickness of a phase plate creates the spiraling phase distribution of an optical vortex. In order to be effective, the phase plate must be smooth and accurately shaped to a fraction of a wavelength. Furthermore, even if it is successfully produced, it is only applicable to one wavelength of light and one topological charge.

A newer, simpler, and more versatile means of creating optical vortices is an adjustable spiral phase plate. In these, the OPL is varied indirectly by *tilting* a surface rather than directly by making it thicker. Adjustable phase plates can be used with multiple wavelengths and can produce a range of topological charges. They may be created by twisting a piece

of cracked Plexiglas and orienting the device so that one tab of the phase plate is directly perpendicular to the incident light, and the other tab is bent at some angle θ away from the other [8]. A laser directed at the end of the crack will then produce an optical vortex because of the azimuthally varying tilt around the center of the phase plate.

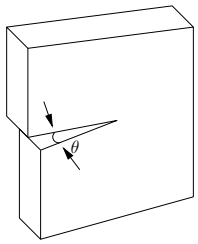

Figure 4: The two sides of the crack in the phase plate are separated by an angle θ.

The phase plate functions on the principle that tilting a transparent object causes a change in optical path length; if the faces are parallel the light, emerges with no angular deviation and just a small displacement. The rate at which OPL changes with the tilt angle starts at zero when the surface is perpendicular to the incident light beam and rapidly increases as indicated by a graph of the derivative of the function below. The derivation of the formula is non-trivial, as it must account for the effects of changing indicies of refraction, but it was achieved independently and found to be in agreement with a similar function in a masters dissertation [9]. Given the scenario in Figure 5, change in optical path length is defined:

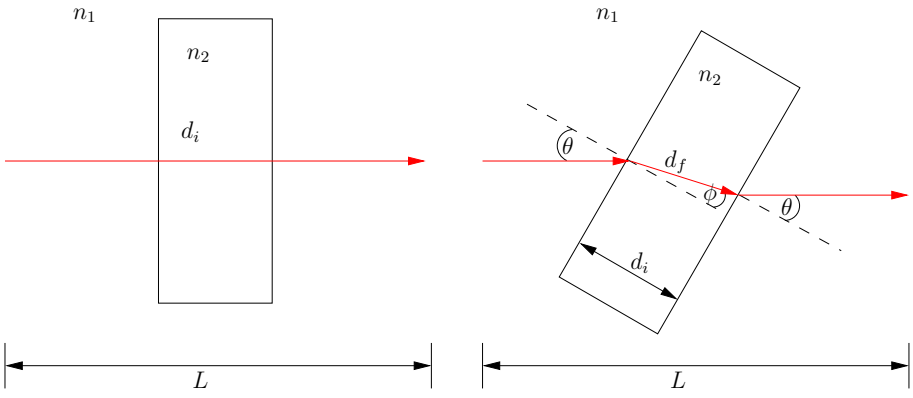

Figure 5: Change in optical path length due to a rotating transparent medium with parallel sides.

$$\Delta\Lambda = d_i \left[n_1 \left(1 - \frac{\cos(\theta - \phi)}{\cos(\phi)} \right) + n_2 \left(\frac{1}{\cos(\phi)} - 1 \right) \right]$$

where ϕ is the angle of refraction given by Snell's law:

$$\sin\phi = \frac{n_1 \sin\theta}{n_2}$$

2.3 Computer Generated Holograms

A picture taken with black and white film records only one facet of a scene: the intensity of light (the square of the amplitude of its electric field). Information about the phase of light, one of the factors that makes objects appear three-dimensional, is completely lost. Holograms offer a means of preserving the phase. In essence, a hologram is just an interference pattern created by a plane reference wave and light scattered off a selected object that is recorded on a photoplate.

A diffraction grating is created by developing the photoplate, and shining the reference beam through this grating exactly reproduces the light, in intensity and phase, that was initially scattered off the object. Looking through the grating provides the illusion that the original object is truly there.

CGHs are used to create optical vortices in precisely the same manner. If the interference pattern between a plane wave and an optical vortex on a photoplate is recorded, and the plane reference wave is shined through the grating, an optical vortex identical to the former one would be generated. A CGH is theoretically produced as follows [10].

The simplest representation of a phase singularity (optical vortex) can be written as

$$E(r, \theta, z) = E_0 \exp(il\theta) \exp(-ikz)$$

where l is the topological charge and θ is an angle in the plane transverse to the direction of propagation. Next, consider a plane wave u, propagating obliquely to the axis

$$u = \exp(-ik_x x - ik_z z)$$

Assume the recording device is located at $z = 0$ for simplicity. The intensity distribution may then be found by squaring the sum of the two amplitude functions:

$$I = 1 + E_0^2 + 2E_0 \cos(k_x x - l\theta)$$

A Fourier transform of this yields the transmittance function actually used to create the diffraction gratings [11]:

$$T(r, \theta) = T_0 \exp\left[i\alpha \cos\left(l\theta - \frac{2\pi}{\Lambda} r \cos\theta\right)\right]$$

where α is the amplitude of the phase modulation, T_0 is the constant absorption coefficient of the hologram, and Λ is period of the grating (fringe spacing).

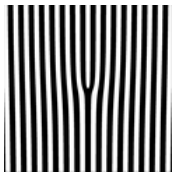

Figure 6: An $l = 1$ grating or the interference pattern created by an oblique plane wave and charge 1 vortex.

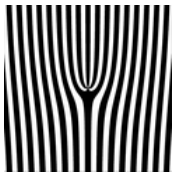

Figure 7: An $l = 4$ grating. Note how there are 4 forks (5 prongs).

Interference patterns between plane waves and collimated optical vortex beams meeting at an angle are characterized by a fork in the center. The charge of the vortex can be determined by counting the number of forks, or subtracting one from the number of prongs. Because these are diffraction gratings, shing a plane wave through one of them will actually create multiple vortices of $\{\ldots, -l, 0, +l, \ldots\}$ charge, where the negative charges have the phase ramp in the opposite direction.

3 The Spiral Phase Plate Vortex Generator

3.1 Materials and Procedures

Standard "unbreakable" plastic cover slips (22 mm square, 0.25 mm thick) were chosen as an alternative material to Plexiglas for the production of spiral phase plates. Attempts to replicate the Technion's method [8] using Plexiglas proved unsuccessful for a number of reasons. The Plexiglass was extremely difficult to crack in a controlled manner and most fractures ocurred arbitrarily. Even if a desirable crack was stumbled upon, the crack tended to propagate while twisting the material, eventually causing the entire piece of Plexiglas to snap in half. In contrast, a cover slip is an inexpensive, optical-quality material that is easily cut with scissors and manipulated without nearly as much concern over durability or crack propagation as Plexiglas. For the experiment, a cover slip was slit radially from the center to a corner. A simple holder was used to keep the phase plate secure and control the angle between the two tabs.

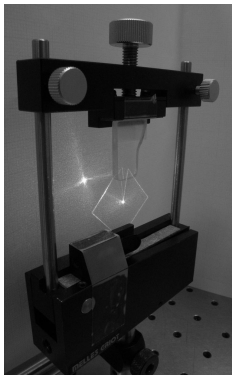

Figure 8: The screw at the top of the holder raises and lowers a piece of Plexiglas into the slit of the cover slip, allowing control over the angle between the two sides.

3.2 The "CJ" Interferometer

The "CJ" interferometer was developed specifically for this project. It is a hybrid between the well-known Mach-Zehnder interferometer and the more elaborate Sagnac [12]. Its advantage over a Michelson interferometer is that the laser never retraces its path, so the laser does not

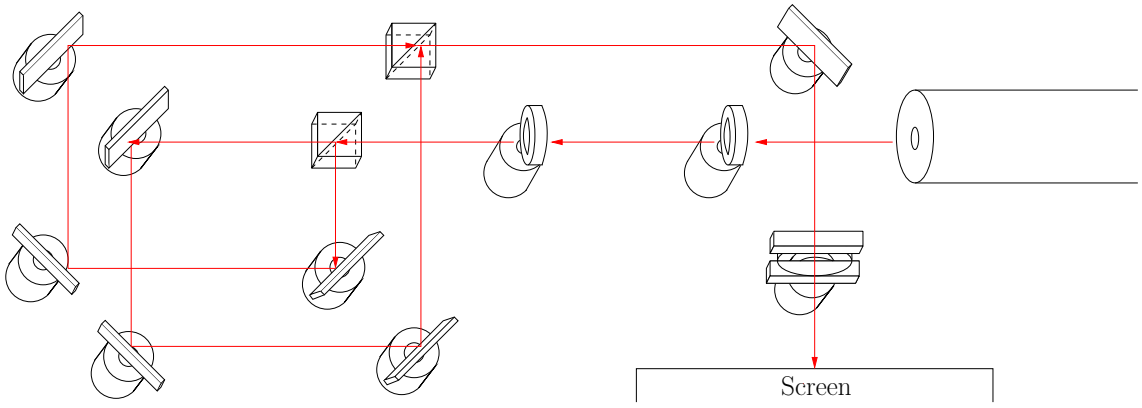

Figure 9: The CJ interferometer. The spiral phase plate is placed in one arm and the resultant optical vortex is interfered with a plane wave from the other arm. The laser is a standard Melles Griot HeNe type, with wavelength λ =632.8 nm. The name CJ is derived from the last name of the author (Jain) and one of his collaborators (Caravelli).

go through the phase plate twice, skewing results. The CJ offers more space than a Sagnac, so placing an object in one arm of the interferometer does not interfere with the path of the laser in the other. The CJ also allows for more spatial control over the beam than the Mach-Zehnder.

Placing the spiral phase plate in one arm of the interferometer resulted in the forked interference patterns (Figures 6 and 7) that are characteristic of optical vortices. Turning the screw on the holder clockwise spread the cover slip's slit further apart, and more forks appeared, indicative of higher order vortices. The device seemed to work well, but understanding it better required a surface scan.

3.3 The Surface Scan

Simple lab equipment and procedures were used to perform the surface scan, which was intended to measure the tilt of the spiral phase plate and thus the phase shift imparted onto a light beam propogating through it. A lens was placed such that the laser beam, once reflected off of a mirror, came to a focus on the spiral phase plate secured in the holder mounted on a two-dimensional translator. Part of the beam reflected off the phase plate and hit the surface of a Plexiglas screen covered with graph paper. The holder was translated in

the horizontal and vertical directions in 0.508 mm (2/100 in) increments over a 10.16 mm by 10.16 mm (0.4 in by 0.4 in) area centered on the middle of the phase plate forming a 21×21 point grid on the cover slip. The position of the laser beam was plotted on the graph paper every time the phase plate was translated. In actuality, only 430 points of data were taken because 11 of the points resided directly on the slit of the phase plate, causing the light to scatter.

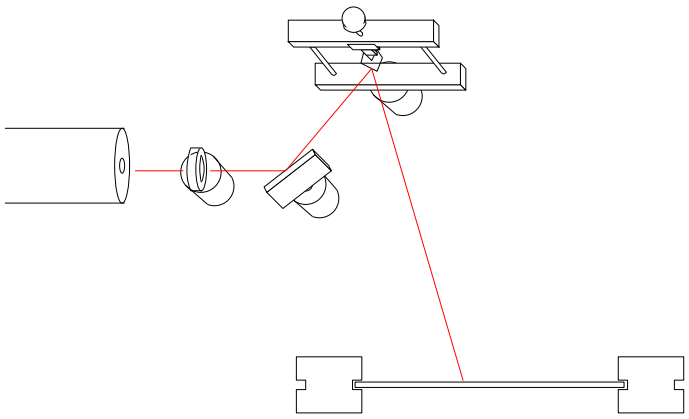

Figure 10: Surface scan setup. Collecting the 430 pts of data and analyzing them took several days

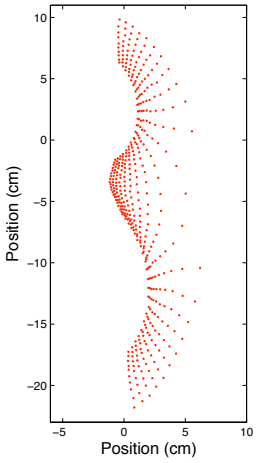

Figure 11: Scatter plot of points reflected off phase plate (origin determined by (x_0, y_0)).

A process was developed to convert the data on the graph paper into the more meaningful values of the x and y tilt of the spiral phase plate. Figure 12 is a closeup schematic diagram of the laser reflecting off the phase plate, which is tilted at some angle $(\theta_{px}, \theta_{py})$. If $\theta_{px} = 0$ (the phase plate is parallel to the initial laser beam and the screen), then the beam will intersect the screen at some x_0, which is used as a reference for all points. Based upon the geometry of the setup, a set of equations were derived to determine the phase plate's tilt as a function of the x and y position of the reflected points on the graph paper (Figure 11):

$$\theta_{px} = \theta_m - \frac{1}{2}\tan^{-1}\left(\frac{L}{x + x_0}\right)$$

and

$$\theta_{py} = \tan^{-1}\left(\frac{y}{L\sqrt{1+\cot^2(2(\theta_m - \theta_{px}))}}\right)$$

The phase shift induced on a light beam depends on the angle between the incident light and the surface normal. Thus, a total tilt θ_t, which describes this angle, is defined as a function of its components θ_x and θ_y by means of a common spherical trigonometric identity to be $\cos(\theta_t) = \cos(\theta_x)\cos(\theta_y)$.

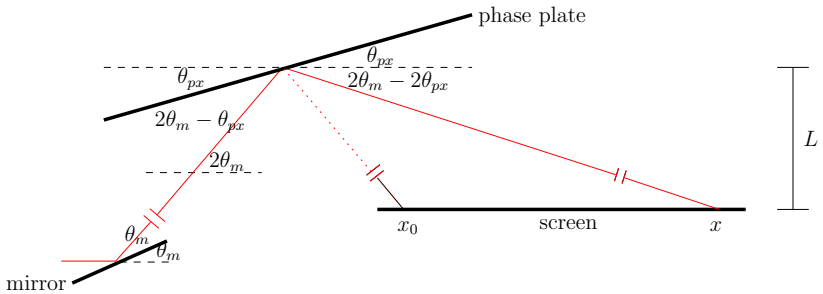

Figure 12: Closeup schematic diagram of laser path during surface scanning.

The x and y coordinates of each data point were read off the graph paper and organized in a spreadsheet. All 430 data points were then translated into their total tilt equivalent via the equations above in Matlab.

3.4 Controlled Tilt Experiment

In order to confirm that the equation relating tilt angle to change in optical path length was derived correctly, an uncut cover slip was placed on a rotation stage in one arm of the interferometer, and the fringes of the interference pattern were projected onto the face of a photodetector (Thorlabs model DET-110). The cover slip was rotated from 90° (perpendicular to the incident light) through 120° at 0.5 degree intervals, and the voltage output from the photodetector was recorded and graphed. Peak voltages indicate the middle of a fringe (a net 2π phase shift, considering the initial 90° position corresponded to the photometer being exposed to the center of a fringe), and voltage minima represent the dark area between fringes (a net π phase shift). One cycle implies a change of λ in optical path length.

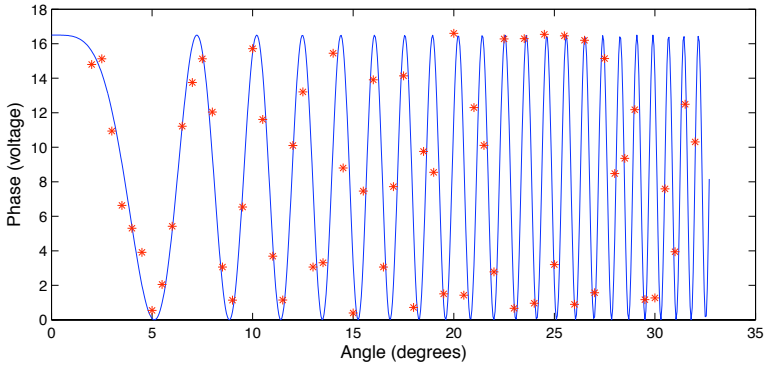

Figure 13: Phaseshift vs. Angle. This curve graphed with $n_1 = 1$, $n_2 = 1.5$, and $d_i = 0.25$ mm.

In the equation from section 2.2.1, $\Delta\Lambda$ may be replaced with $m\lambda$, so that the change in optical path length is represented by some m number of wavelengths. Dividing both sides by λ yields an approximately parabolic curve that relates $\Delta\Lambda$ in wavelengths to the tilt angle θ. In order to achieve the cyclical pattern demonstrated by the data, it is only needed to take the cosine of the function and multiply the argument by 2π:

$$p(\theta) = \cos\left(2\pi\frac{d_i}{\lambda}\left[n_1\left(1 - \frac{\cos(\theta-\phi)}{\cos(\phi)}\right) + n_2\left(\frac{1}{\cos(\phi)} - 1\right)\right]\right)$$

The theoretical model fits the experimental graph quite nicely and confirms not only the derivation of the function, but also a direct measurement of d_i, the thickness of the cover slip. It is important to note that the more tilted the phase plate was, the less additional rotation was necessary to produce any given phase shift. That is why the data points on each cycle get succesively scarcer. Note that the function actually graphed was $k(p(\theta)) + 1)$, where $k = 8.25$ in order to fit the curve to the voltages measured by the photodetector.

3.5 Phase Analysis

The function above was used to associate all 430 data points of θ_t with a phase shift in Matlab, a computer program for numerical analysis. Figure 14 contains a plot of θ_t against position on the phase plate, and a map of the phase of light leaving the spiral phase plate. The slit is represented on the right side by a line of 11 uniformly colored squares. The color

of the figure is mostly constant along any given radius, confirming that the phase shift is azimuthally dependent (holding the paper farther back may help to see this more easily). A change in color from light to dark to light or dark to light to dark indicates a phase shift of 2π. The phase map suggests that the phase plate is set for creating an $l = 8$ or $l = 9$ vortex. In the area directly left of the slit, the phase pattern is slightly distorted. Most likely, this may be attributed to irregular twisting of the left tab by the Plexiglas wedge.

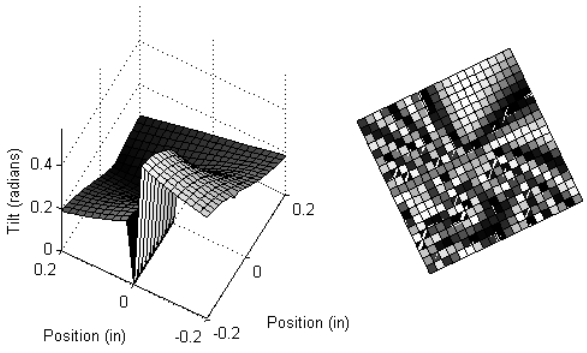

Figure 14: The points of constant phase extend radially in accord with true vortex structure.

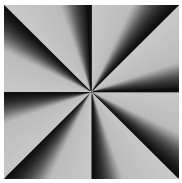

Figure 15: The ideal phase distribution for an $l = 8$ vortex.

3.6 Intensity Distribution

In addition to a spiral phase structure, optical vortices must also possess a doughnut-shaped intensity distribution. The intensity distribution of an $l = 1$ vortex was measured by taking an uncompressed, black and white intensity image with a digital camera and analyzing it in Matlab.

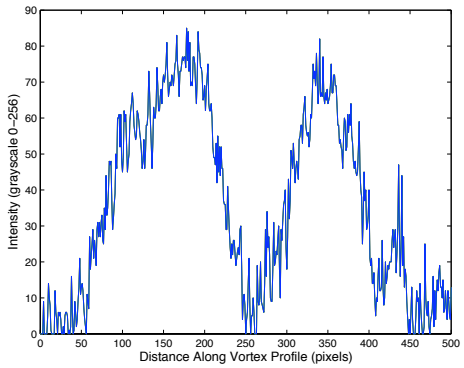

Figure 16: Intensity profile of optical vortex created by spiral phase plate. The linear, wedge-shaped intensity distribution near the center of the profile is consistent with $l = 1$.

4 Vortex Analyzer

4.1 Composite Grid CGHs

CGHs are an alternative method for creating optical vortex beams, but they may also be used to analyze them. Shining an optical vortex of the same topological charge as the one used to create the CGH will produce a plane wave. In order to test a beam for its topological charge, one could theoretically shine the beam through an $l = 1$ grating, an $l = 2$ grating, an $l = 3$ grating, ... and the grating that produced a plane wave output would correspond to the l-value of the vortex beam. It is possible, however, to speed up this process by using the principle of conservation of topological charge [13], which essentially states that the topological charge of a composite vortex is the sum of the charges of its components. Therefore, one could superimpose two orthogonal CGHs and create composite vortices of a range of topological charges.

Shining a plane wave through Figure 19 would create vortices ranging from $l = -4$ to $l = +4$. As a result, this grating is also capable of analyzing vortices of the same charge range. For example, shining an $l = -3$ vortex through this grid would cause a plane wave beam (Gaussian intensity distribution) to appear in the spot a charge -3 vortex would normally be in under the condition of an incident plane beam.

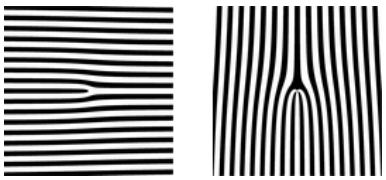

Figure 17: Left: $l = 1$ grating. Right: $l = 3$ grating.

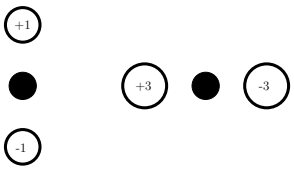

Figure 18: Vortices and topological charges created by respective gratings in Figure 17.

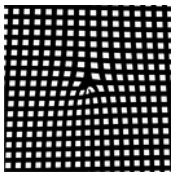

Figure 19: Composite grid CGH ($l = 1$ and $l = 3$ superposition).

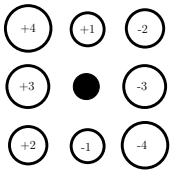

Figure 20: Resultant vortex and topological charge layout.

4.2 Materials and Procedures

A modified version of the transmittance function from section 2.3 (adjusted for Cartesian coordinates) was used in Matlab to create the CGHs. The function was calculated for 1800 $\times$ 1800 points in a 16 $\times$ 16 unit square centered on the origin. The fringe spacing was set to 1. The image created was exported from Matlab and cropped in The Gimp (image editing software) to 2934 $\times$ 2934 pixels. It was reduced to 120 $\times$ 120 pixels in ImageMagick and then printed at 10% its size onto common transparency paper at 600 dpi by a laser printer.

Previous methods for creating CGHs involved taking a film photograph of a large printout of the desired design, then having it developed and photoreduced into a slide from the negatives. This is a costly and tedious process. It is also possible to test grating designs immediately with a device called a spatial light modulator, which can adjust the intensity and/or phase of light using a small, high resolution lcd display, but this is even more costly, at thousands of dollars. The procedure developed above is both inexpensive and immediate, and marks a further simplification of the methods used to create optical vortices.

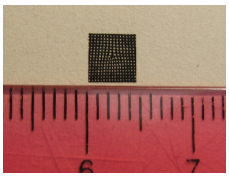

Figure 21: Actual CGH next to ruler for scale.

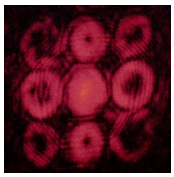

Figure 22: Actual vortices created by grid CGH.

5 The OAM Sorter Concept

An conceptual method for sorting vortex beams by their OAM was developed with two components, spiral phase plates and composite grid CGHs, and a novel combinatoric approach to increasing the alphabet of states available for data transmission. The concept entails using multiple vortex generators in conjunction with one vortex analyzer.

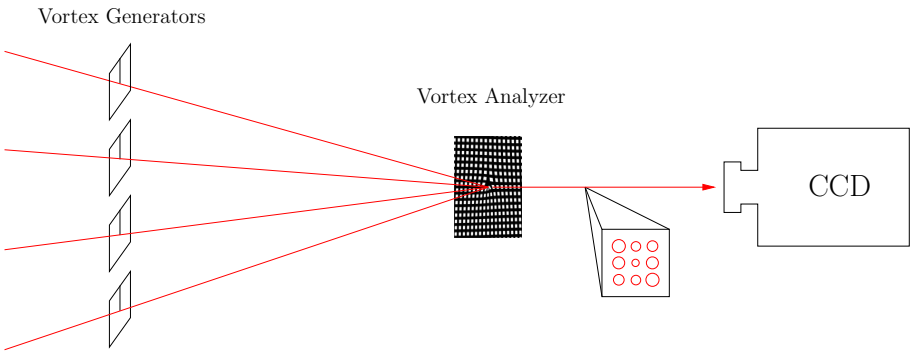

Figure 23: The OAM sorter schematic with 4 vortex generators.

The beams incident on the spiral phase plates have distinct frequencies, so they do not interfere with each other when they coincide at the grid CGH. The angle between the various rays should be minute. The resultant diffraction pattern is then captured by a CCD camera, where it is analyzed for intensity.

If there were only one vortex generator, then the alphabet would be limited to 8 states (assuming the usage of the grid CGH above, which can test for up to 8 states simultaneously). If there are two independent vortex generators, then the alphabet is increased to 36 states (e.g. the two l-states can be (-4,-4), (-3,1), (2,3)...). If the generators produce vortices of the same topological charge (e.g. (-4,-4)), the CCD camera will record a plane wave of twice the intensity of the incident beams in the -4 slot of the grid. This can be mathematically modelled as a combination-with-repitition problem so that the function describing the total number of states S is given by:

$$S = \frac{(t+g-1)!}{g!(t-1)!}$$

where t is the number of toplogical charges that can be tested for and g is the number of vortex generators. The potential of this method becomes apparent when increasing the number of vortex generators.

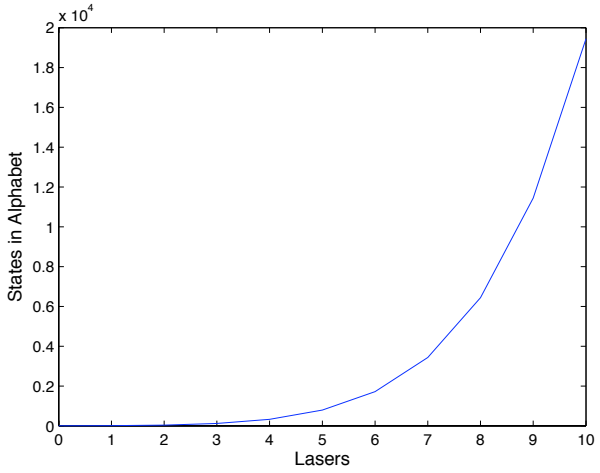

Figure 24: Number of possible information states vs. number of vortex generators.

g	S
1	8
2	36
3	120
4	330
5	792
6	1716
7	3432
8	6435
9	11440
10	19448

Figure 25: Table of Figure 24.

Figure 24 is for $t = 8$. As g increases, the number of states rapidly escalates. With only 10 vortex generators, it is possible to transmit any one of 19,448 states. With 15 generators, the alphabet is over 170,000. This represents a significant improvement over conventional binary data transfer, which allows only two states.

6 Conclusion

The adjustable spiral phase plate constructed from a plastic microscope cover slip was demonstrated to be an effective means of producing optical vortices, which can be used to encode information into light beams. The phase plates produced are inexpensive and 100% efficient, making them suitable for applications that require high-intensity beams such as optical tweezers. The phase distribution of the vortices produced was successfully mapped by performing a surface scan of the phase plate, and intensity profile measurements confirmed vortex characteristics. A simplified method for analyzing optical vortices using computer-generated holograms was also developed and implemented in the form of a composite vortex grid.

These two components were then integrated in a conceptual OAM sorter that employs a novel combinatoric transmission method to increase the alphabet of states used for data transmission thousands of times over traditional binary methods. Although the sorter requires improvements before becoming practical for actual usage, it demonstrates the promise of using the orbital angular momentum of photons for high-speed data transfer.

7 Acknowledgements

I would like to thank Dr. John Noé and Prof. Harold Metcalf of the Laser Teaching Center at Stony Brook University for their efforts and insights. I thank Greg Caravelli of John Hopkins University, who was a collaborator in the spiral phase plate portion of the project. In addition, I would like to recognize the other students of the LTC, Azure Hansen of Stony Brook , Dr. Marty Cohen , and Prof. Kiko Galvez of Colgate University. This research was supported by the Simons Foundation and NSF Grant No. PHY-0243935.

References

[1] M. D'Amico, A. Leva, B. Micheli, "Free-space optics communication systems: First results from a pilot field-trial in the surrounding area of Milan, Italy," *IEEE Microwave and Wireless Components Lett.* **13**, 305 (2003).

[2] L. Allen, M. W. Beijersbergen, R. J. C. Spreeuw, J. P. Woerdman, "Orbital angular momentum of light and the transformation of Laguerre-Gaussian laser modes," *Phys. Rev.* A **45**, 8185 (1992).

[3] J. Leach, M.J. Padgett, S. M. Barnett, S. Franke-Arnold, J. Courtial, "Measuring the orbital angular momentum of a single photon," *Phys. Rev. Lett.* **88**, 257901 (2002).

[4] J. F. Nye, M. V., Berry, "Dislocations in wave trains," *Proc. Roy. Soc. Lond.* A **336**, 165 (1974).

[5] J. Arlt, K. Dholakia, L. Allen, and M. J. Padgett, "The production of multiringed Laguerre-Gaussian modes by computer-generated holograms," *J. mod. Opt.* **45**, 1231-1237 (1998).

[6] M. W. Beijersbergen, L. Allen, H. E. L. O. van der Veen and J. P. Woerdman, "Astigmatic laser mode converters and transfer of orbital angular momentum," *Opt. Commun.* **96**, 123-132 (1993).

[7] G. Gibson, J. Courtial, M.J. Padgett, M. Vasnetsov, V. Pas'ko, S. M. Barnett, and S. Franke-Arnold, "Free-space information transfer using light beams carrying orbital angular momentum," *Opt. Express* **12**, 5448-5456 (2004).

[8] C. Rotschild, S. Zommer, S. Moed, O. Hershcovitz and S. G. Lipson, "Adjustable spiral phase plate," *Appl. Opt.* **43**, 2397-2399 (2004).

[9] M. Merschdorf. Masters dissertation, Stony Brook University, 1995.

[10] H. He, N. R. Heckenberg, H. Rubinsztein-Dunlop, "Optical particle trapping with higer-order doughnut beams produced using high efficiency computer generated holograms," *J. Mod. Opt.* **42**, 217-223 (1995).

[11] C.-S. Guo, X. Liu, X.-Y. Ren, H.-T. Wang, "Optimal annular computer-generated holograms for the generation of optical vortices," *J. Opt. Soc. Am.* **22**, 385-390 (2005).

[12] E. Hecht, *Optics, 3rd Edition* (Addison Wesley Publishing Company, 1997)

[13] M. S. Soskin, V. N. Gorshkov, M. V. Vasnetsov, J. T. Malos, N. R. Heckenberg, "Topological charge and angular momentum of light beams carrying optical vortices," *Phys. Rev.* A **56**, 4064-4075 (1997).